Concept of a laser-plasma-based electron source for sub-10-fs electron diffraction

J. Faure,* B. van der Geer, B. Beaurepaire, G. Gallé, A. Vernier, and A. Lifschitz

LOA, ENSTA ParisTech, CNRS, Ecole polytechnique, Université Paris-Saclay, Palaiseau, France

(Received 14 October 2015; published 19 February 2016)

We propose a new concept of an electron source for ultrafast electron diffraction with sub-10-fs temporal resolution. Electrons are generated in a laser-plasma accelerator, able to deliver femtosecond electron bunches at 5 MeV energy with a kilohertz repetition rate. The possibility of producing this electron source is demonstrated using particle-in-cell simulations. We then use particle-tracking simulations to show that this electron beam can be transported and manipulated in a realistic beam line, in order to reach parameters suitable for electron diffraction. The beam line consists of realistic static magnetic optics and introduces no temporal jitter. We demonstrate numerically that electron bunches with 5-fs duration and containing 1.5 fC per bunch can be produced, with a transverse coherence length exceeding 2 nm, as required for electron diffraction.

DOI: 10.1103/PhysRevAccelBeams.19.021302

I. INTRODUCTION

In the past decade, there has been great progress in plasma-based techniques for accelerating particles [1]. In particular, in laser-plasma accelerators, an ultraintense laser pulse drives a relativistic electron plasma wave—or wakefield—in the plasma. The wakefield is an accelerating structure with extremely high accelerating gradients, on the order of 100 GV/m, and is able to accelerate electrons to relativistic energies in micrometer distances. Currently, laser-plasma accelerators provide electron beams ranging from hundreds of MeV [2–4] to multi-GeV energies [5,6] and charges in the tens of picocoulomb range. Numerous methods have been developed to control the injection of electrons into the wakefield [7–11], resulting in energy spreads at the few percent level [12]. In addition, when the injection is done properly, femtosecond electron bunches can be generated: in Ref. [13], an 80 MeV electron beam with 1.5-fs rms duration was experimentally demonstrated. This emerging technology holds the promise of compact particle accelerators delivering high charge femtosecond bunches with intrinsic synchronization to an optical pulse. Jitter-free synchronization originates from the fact that the accelerating structure is directly driven by the laser. Therefore, temporal jitter should not be of concern, and sub-10-fs temporal resolution should be attainable in experiments. These unique properties make laser-plasma accelerators attractive for applications requiring femtosecond bunches and high peak currents, such as the development of compact free electron lasers (FELs) [14–16].

Recently, ultrafast electron diffraction (UED) [17] has emerged as a powerful, compact, and cost-effective technique for studying ultrafast structural changes in solids, gases, or liquids [18,19]. However, the time resolution in UED experiments has been limited to > 100–200 fs, either because of space charge [19] or rf jitter [20,21]. Reducing the temporal resolution to the sub-100-fs range and even the sub-10-fs range, remains a challenge of importance as it could give access to the observation of new phenomena and new physics in pump-probe experiments.

In this article, we use numerical simulations to show that a laser-plasma accelerator can provide an electron source well suited for UED with sub-10-fs resolution. The laser-plasma accelerator we have designed is able to produce picocoulomb of charges in the 5 MeV range and with a < 10-fs bunch duration. In Sec. II, we use particle-in-cell (PIC) simulations to show that such bunches can be generated at a kilohertz repetition rate. In Sec. III, we tackle the problem of beam transport of the electron source: we design a beam line which produces a high-quality beam (small transverse emittance, narrow energy spread) with sub-10-fs duration at the sample position, tens of centimeters downstream of the electron source. Beam transport of laser-driven electron beams has been studied in the context of a driver for a FEL [14,16] but not as a driver for a UED experiment. Finally, Sec. IV shows results of the beam line optimization using the general particle tracer (GPT) code [22]. We show that the beam line is able to provide $\simeq$5-fs bunches with femtocoulomb charge and normalized transverse emittances of $\varepsilon_{n\perp} \simeq 10$–$20$ nm.

*Corresponding author.
jerome.faure@ensta.fr

II. LASER-PLASMA ELECTRON SOURCE

Electrons are produced during the interaction of an ultraintense and ultrashort laser pulse with an underdense plasma. The ultraintense laser pulse perturbs the electron density via the ponderomotive force and excites a large-amplitude plasma wave, in which electrons can be trapped. The maximum energy that electrons can gain in this process is given by $\Delta E \propto mc^2\gamma_p^2\delta n/n_0$, where m is the electron mass, c is the velocity of light, $\delta n/n_0$ is the amplitude of the plasma wave, and $\gamma_p = (n_c/n_0)^{1/2}$ is the Lorentz factor corresponding to the plasma wave phase velocity v_p, with n_c and n_0, respectively, the critical density and the electron plasma density. Therefore, at high density $n_0/n_c \simeq 0.1$ (i.e., $n_0 \simeq 10^{20}$ cm^{-3}), plasma accelerators can produce electrons at about 5–10 MeV, a range suitable for electron diffraction [23–25].

Previous experiments in the self-modulated laser wakefield have shown that using a 30-fs, high-energy laser pulse ($\simeq$1 J) in a high-density plasma can lead to copious amounts of electrons in the 1–10 MeV range [26]. Electrons were self-injected [26] or injected through ionization [27], and the obtained bunches did not have femtosecond durations but rather tens of femtoseconds. In addition, the beam quality was rather poor with a large energy spread and a large divergence. Higher-quality bunches can be generated in the *bubble regime* [28], which is obtained when the laser pulse length is matched to the plasma wavelength. In this regime, the laser pulse ponderomotive force drives a nonlinear plasma wave in which electrons form a spherical electron sheath around the ions (the so-called plasma bubble). In this case, electrons can be trapped into this spherical bubble, leading to a divergence in the range of a few millirads, an energy spread of 1%–10% and a duration of a few femtoseconds [2,13].

The bubble regime can be obtained for a given set of laser and plasma parameters [29], the basic idea being that the laser pulse is matched longitudinally and transversely to the plasma wave. Assuming that R is the size of the spherical bubble, the longitudinal matching condition can be written as $c\tau \simeq R/2$, where τ is the laser pulse duration. The transverse matching condition reads $k_pR = 2\sqrt{a_0}$, where $a_0 = eA_0/mc\omega_0$ is its normalized vector potential and $k_p = \omega_p/c$ is the plasma wave vector. From these simple considerations, scaling laws [29] show that electrons can be accelerated in the 10 MeV range using a 5-fs laser pulse with $\simeq$5 mJ and focused to a $w_0 = 2.5$ μm waist.

Few-millijoule and few-cycle ($\sim$5-fs) laser pulses are currently obtained in state-of-the-art kilohertz laser systems [30,31]. The high repetition rate of the millijoule lasers is a great advantage for pump-probe experiments compared to joule-level laser systems operating at 10 Hz or less. Indeed, UED requires the detection of changes at the percent level in the intensity of the Bragg peaks and averaging data at kilohertz helps to increase the statistics and wash out the charge fluctuations inherent to plasma accelerators. Note that laser-plasma accelerators operating at a kilohertz repetition rate were recently demonstrated [32] as well as their application to electron diffraction [33]. Higher stability was observed in these high repetition rate experiments. However, the electrons were accelerated in the 100 keV range, and the bunch length quickly stretched due to velocity dispersion. Recently, there has been intense research in the development of 10 MeV, high-charge femtosecond bunches [34,35], but to date, the experimental demonstration of a kilohertz laser-plasma accelerator delivering MeV and femtosecond electron bunches is still pending.

The laser-plasma interaction was modeled using the fully electromagnetic PIC code Calder-Circ which provides a quasi-3D geometry [36]. Simulations used realistic experimental parameters, namely, a 5-fs full width at half maximum (FWHM) pulse centered around $\lambda_0 =$ 800 nm with an energy of 4.1 mJ. The pulse is propagating in an underdense plasma, whose longitudinal density profile consists of a 203 μm plateau preceded and followed by a 63 μm ramp. The electronic density on the

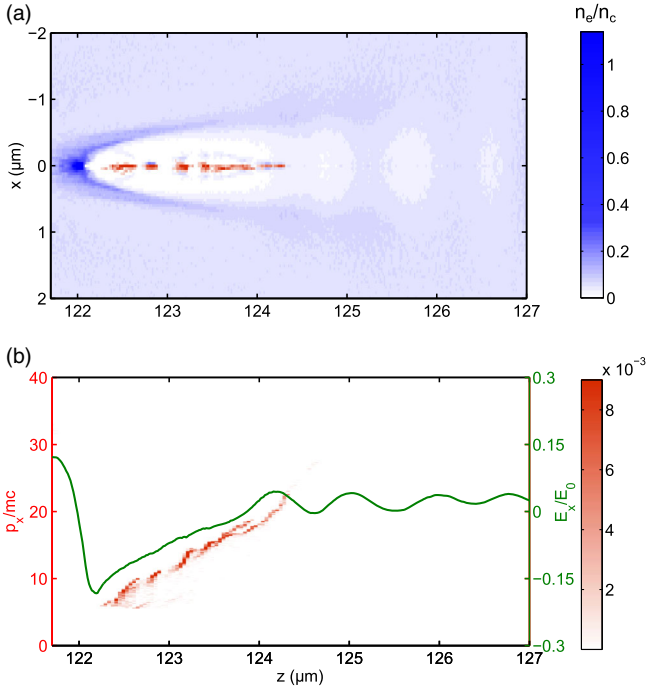

FIG. 1. Results of PIC simulations. (a) Map of the electron density in the plasma (n_e/n_c blue color bar): the 5-fs laser pulse drives a plasma cavity, in which high-energy electrons are accelerated (red color bar). (b) Longitudinal phase space density map showing an accelerated electron bunch with energy in the 5–10 MeV range. The green curve is the wakefield longitudinal electric field originating from the plasma cavity.

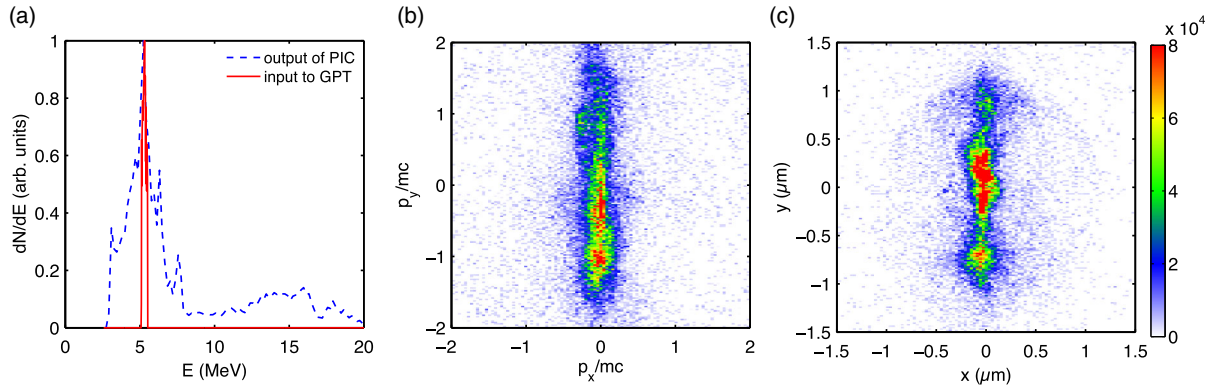

FIG. 2. Results from PIC simulations. (a) Blue line: Electron energy distribution at the output of the PIC code. Red line: The filtered energy distribution ($\delta E/E = 2\%$) which is used as an input of the particle transport code (GPT). (b) Electron distribution in transverse phase space (p_x, p_y) and (c) in real laboratory space (x, y). Both plots show an elongation of the distribution along the direction of laser polarization.

plateau is $n_0 = 0.05 \times n_c = 8.7 \times 10^{19}$ cm^{-3}. The laser beam is focused at the beginning of the plateau, down to a waist of 4.3 μm, so that the laser intensity is $I = 2.6 \times 10^{18}$ W/cm^2—the corresponding value of the normalized vector potential is $a_0 = 1.1$. The laser is polarized along the y axis and propagates along the z axis. The box is composed of 1500×200 cells with 220 particles per cell. The longitudinal cell size is $0.125c/\omega_0$, and the radial cell size is $0.628c/\omega_0$. The physics of this interaction was studied in detail in a previous publication [37]. We showed that the highly nonlinear evolution of the laser pulse causes the slowdown of the wakefield whose phase velocity becomes subrelativistic. Electrons are then injected in this "slow" wakefield and accelerated to energies in the 5–10 MeV range. Figure 1(a) shows the electron density in the plasma. One can clearly see the plasma bubble (blue color bar) and the electron bunch (in red) which is injected and accelerated into it. In Fig. 1(b), the electron bunch is represented in the phase space (z, p_z). Electrons are accelerated at the 5–10 MeV level, and the bunch spreads over 2 μm, i.e., $\simeq$6 fs. Figure 2(a) shows the electron energy distribution when the electron beam exits the plasma. The distribution (dashed blue line) has a relatively large peak at 5 MeV ($\delta E/E = 23\%$ at FWHM) and contains 7 pC of charge. The red line shows the distribution which was trimmed to a smaller energy spread $\delta E/E = 2\%$ FWHM and still contains a charge of $\sim$1 pC (this trimmed distribution is used for the design of the beam transport system in the following section). Figure 2(b) shows the electron distribution in transverse phase space (p_x, p_y). The transverse momentum is much larger in the direction of the laser polarization (y direction), indicating the electron beam has gained more momentum in this direction because of its direct interaction with the laser field. A similar behavior is seen in Fig. 2(c), which represents the beam distribution in (x, y): the beam is more elongated along the y axis. Note the very small source size, $\sigma_x \simeq 0.1$ μm in the x direction. The normalized rms emittance of this beam is $\varepsilon_x = 10$ nm and $\varepsilon_y = 300$ nm (including the useful part of the charge, i.e., 75% of the total charge; see Table I for more details). Even though the transverse emittance is good, the beam has a large divergence $\theta_x = 15$ mrad and $\theta_y = 80$ mrad.

TABLE I. Parameters of the various distributions used in this work. Row 1: A distribution that models the PIC distribution shown in Fig. 2. The distribution is uniform; thus, the σ values correspond to the width of uniform distributions. Row 2: Parameters of the output distribution through the beam line when the model distribution is used (as in Figs. 5 and 6). Row 3: Parameters of the distribution from the PIC simulations shown in Fig. 2. Note that the energy spread was trimmed to 2% at FWHM for making computing in the particle-tracking simulations easier. Row 4: The resulting distribution at the sample plane obtained when the PIC distribution is used. For rows 2–4, the various σ represent the rms values of the distributions.

Distribution	Charge (fC)	γ_0	σ_γ/γ_0 (%)	σ_x (μm)	σ_y (μm)	σ_{p_x} (mc)	σ_{p_y} (mc)	ε_{nx} (nm)	ε_{nx} (nm)	L_{cx} (nm)	L_{cy} (nm)
Model (uniform)	500	10.3	4.8	0.2	1	0.1	1	1.6	83	⋯	⋯
At sample plane (from model)	2.8	10.3	0.3	150	200	2×10^{-3}	2×10^{-4}	15	40	4	2
Input distribution from PIC	770	10.3	1.2	0.1	0.6	0.1	0.6	8	300	⋯	⋯
At sample plane (from PIC)	1.2	10.3	0.3	145	200	2×10^{-3}	2×10^{-4}	15	50	4	2

III. BEAM LINE DESIGN

The electron beam described in the previous section cannot be used directly for electron diffraction for several reasons. First, the diffraction sample has to be placed sufficiently far away from the source so that it does not get damaged by the laser pulse which generates the electron beam. This implies that the electron beam has to propagate tens of centimeters before reaching the sample. Since the energy spread is quite large, the bunch duration increases upon a vacuum drift of length L_d. For a relativistic beam with $\gamma^2 \gg 1$, the bunch stretches by dt:

$$dt = \frac{L_d}{c}\frac{\delta\gamma}{\gamma^3}. \tag{1}$$

For example, after a 20 cm propagation, a 5 MeV bunch with an energy spread of 2% will stretch by 130 fs. Similarly, energy fluctuations of 2% will translate to a temporal jitter of 130 fs. The bunch emerging from the laser plasma interaction has a 20% energy spread and is likely to fluctuate in energy. To maintain the sub-10-fs duration, the beam line should satisfy the following conditions: (i) restrict the energy spread to the 1% level, (ii) fix the absolute energy in order to avoid energy fluctuation which would degrade the temporal resolution by introducing a temporal jitter, and (iii) recompress the electron bunch duration at a given position, tens of centimeters away from the source.

In order to obtain high-quality diffraction images, the beam should also have a very good transverse emittance. Electron diffraction is a single electron phenomenon: constructive interference in the direction of the Bragg angles will occur only if the electron wave packet has a large transverse coherence L_{cx} (along x). The transverse coherence is related to the beam transverse normalized emittance by

$$L_{cx} = \frac{\hbar}{mc}\frac{\sigma_x}{\epsilon_{nx}}, \tag{2}$$

where σ_x is the rms beam size along x. Typically, L_{cx} should be larger than the size of the unit cell of the crystal under consideration. For instance, taking $L_{cx} > 1$ nm and $\sigma_x = 100\ \mu$m implies a very good emittance: $\epsilon_{nx} < 30$ nm. Therefore, the beam line should be able to maintain the beam emittance while providing the correct beam size, $\sim$100 μm on the sample. Finally, other design considerations were taken into account: (i) compacity of the beam line, length < 1 m, and (ii) no rf elements in order to avoid time jitter which would spoil the temporal resolution.

Such a beam line is not standard, especially when considering the sub-10-fs target for the bunch duration. In particular, it is desirable that the compression be performed using a magnetic bunch compressor in order to avoid temporal jitter [38,39]. The idea of the beam line is presented in Fig. 3: the first pair of quads is used to focus the beam into the bend magnet, while the second pair of quads is used to adjust the beam size in the sample plane. The 45° bend magnet provides compression of the bunch but also disperses it in the x plane so that, using a slit, the central energy and the energy spread can be tuned. The first slit is used to trim the angular distribution, while the second restricts the beam size and the energy spread. Note that the whole beam line fits within 50 cm.

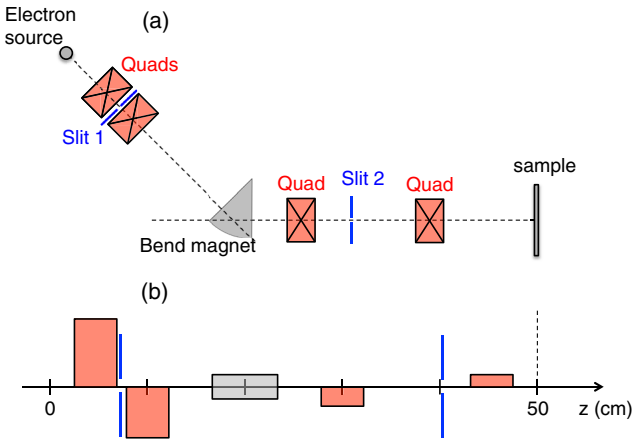

FIG. 3. (a) Schematic representation of the static compression beam line. Note the presence of two slits which are used to trim the electron distribution. (b) Conventional representation of the beam line showing the distance between magnetic elements: one-half of each quadrupole magnet is depicted, above the beam center line for a converging lens (in the x plane) and below the center line for a diverging lens. The sample plane lies at $z = 50$ cm.

For such short bunches, there are large spatiotemporal couplings that appear during propagation in the beam line. Electrons traveling with larger angles fall at the back of the bunch, and it is not possible to recompress the bunch when the electron source has a large divergence angle. To model bunch dynamics in the beam line, we used a ray-tracing model where magnetic optics are described in the framework of the hard edge approximation [40]. The initial conditions of an electron are represented by a vector $\mathbf{v_0} = (dx, \theta_x, dy, \theta_y, dl, dp/p_0)$ where all components of $\mathbf{v_0}$ are taken with respect to the central trajectory $\mathbf{v_0} = 0$. For instance, dp/p_0 is the relative momentum displacement of the electron, and dl is the path length difference with respect to the reference electron. One can obtain information on the temporal displacement of electrons by writing that $dt = dl/v$, where v is the electron velocity. Transport through the beam line is described by equation $\mathbf{v} = M\mathbf{v_0}$, where M is a 6×6 matrix representing all magnetic elements.

Let us first consider longitudinal dynamics in the bend magnet, i.e., $dx \ll 1$ and $\theta_x \ll 1$. From the bend magnet matrix, one can easily show that a bunch is longitudinally recompressed after a drift corresponding to the temporal focal length of the bend magnet:

$$f_{\text{bend}} = (\alpha - \sin\alpha)\frac{mc}{eB_0}\gamma^3 \tag{3}$$

where e is the electron charge, α the bending angle, and B_0 the bending magnetic field. With the parameters of our beam line ($\alpha \simeq 45°$ and $B_0 = 0.35$ T), this implies that the bend magnet can compensate a drift of $L_d = f_{\text{bend}} = 45$ cm, which defines the total length of the beam line.

This analysis does not hold when considering transverse effects: a finite dx and a finite angle θ_x also contribute to the temporal shift of the trajectory. In this case the temporal shift in the bend dt reads

$$vdt = dx\sin\alpha + (1-\cos\alpha)\rho_0\theta_x + (\alpha - \sin\alpha)\rho_0\frac{dp}{p_0}, \tag{4}$$

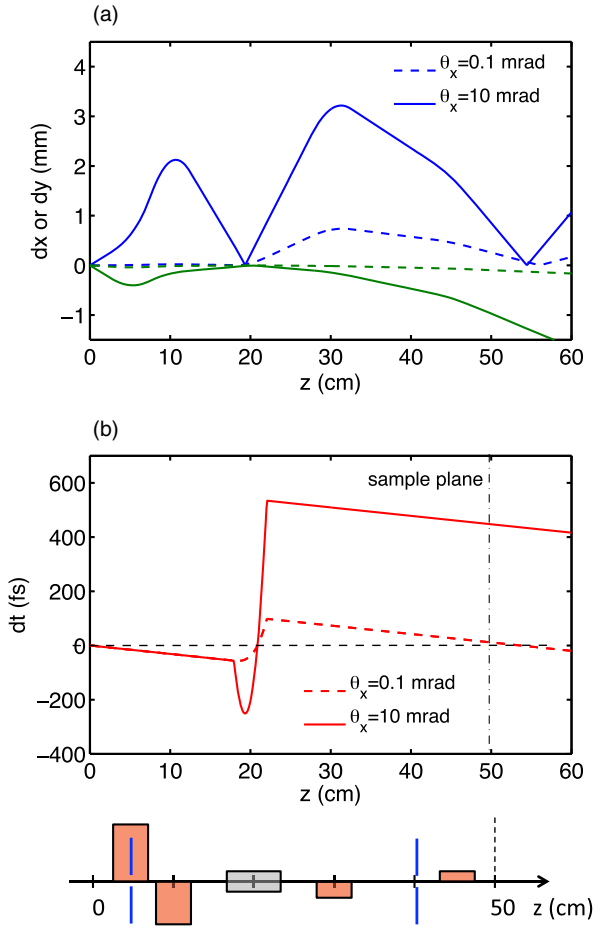

FIG. 4. Ray-tracing model showing electron trajectories through the beam line. (a) Blue lines (green line): Relative displacement dx (dy) with respect to the central trajectory. These trajectories originate from the axis $dx = dy = 0$ and have initial divergences $\theta_x = \theta_y = 10$ mrad (full line) and $\theta_x = \theta_y = 0.1$ mrad (dashed line); their momentum is shifted $dp/p_0 = 1\%$. (b) Relative time displacement $dt \simeq dl/c$ for the same trajectories. Bottom: Schematic of the beam line.

where $\rho_0 = p_0/eB_0$ is the radius of curvature of the central trajectory in the bend. When these transverse terms are large, the bend does not recompress the bunch correctly. These transverse effects can be neglected when

$$dx \ll \frac{\alpha - \sin\alpha}{\sin\alpha}\rho_0\frac{dp}{p_0}, \tag{5}$$

$$\theta_x \ll \frac{\alpha - \sin\alpha}{1-\cos\alpha}\frac{dp}{p_0}. \tag{6}$$

With our parameters, transverse effects in the bend magnet can be neglected if $dx \ll 50\ \mu$m and $\theta_x \ll 2$ mrad, explaining why large divergence angles are not acceptable to achieve recompression. Our beam line design ensures that dx is small by focusing the beam inside the bend magnet, and the reduction of the divergence is achieved by spatial filtering with the two slits.

These effects can be quite dramatic, as can be seen in Fig 4: for the low divergence case, transverse effects are negligible and the bend recompresses the bunch ($dt = 0$) at the sample plane: $z = f_{\text{bend}} = 50$ cm. This is not the case for a large divergence: in this case, the duration reaches ~500 fs in the sample plane. We conclude that the beam line is suitable for recompressing the electron bunch provided that slits are used to trim the angular distribution, which comes at the expense of a large loss of beam charge.

IV. NUMERICAL SIMULATIONS OF THE BEAM TRANSPORT

The optimization of this beam line is complex, because it needs to take into account multiple and potentially conflicting objectives. Indeed, the beam line has to deliver at the sample plane (i) a narrow energy spread beam, (ii) a small beam size ~100 μm, (iii) a large coherence length > 1 nm, (iv) the shortest bunch duration, and (v) the largest amount of charge. To solve this problem, we used a genetic algorithm in the GPT code to find the optimum parameters of the beam line. The genetic algorithm assigns random values to a set of free parameters in the beam line, namely, the quadrupole field strength, the size of the slits, and the bend angle. First, a large number of beam line configurations are generated randomly. GPT is then used to propagate the electron beam through all configurations and to estimate the beam parameters in the sample plane, computing several figures of merit for assessing the beam quality. The results are then ranked according to these figures of merit, the best results are selected for producing new configurations, and the algorithm proceeds to a new iteration. Concerning beam transport modeled by GPT, all magnetic elements include fringe fields [41]. All beam line components are realistic off-the-shelf magnets; for example, the gradient in the quadrupoles are all < 20 T/m, and the magnetic field of the bending magnet is modest: 0.35 T. Space charge is not taken into account for the

optimization with the genetic algorithm in order to keep computational time to a reasonable level. For the optimization, we used a simplified model distribution which approaches the electron distribution given by the PIC simulations as described in Sec. II—see also Table I for all details on this model distribution.

Figure 5 shows the results of a genetic optimization of the beam line. In Fig. 5(a), each point represents a beam line configuration in a plot of rms duration σ_t versus charge. This plot shows that femtocoulomb bunches with sub-10-fs duration can be obtained, which is a remarkable result. Indeed, femtocoulomb charge at a kilohertz repetition rate permits one to obtain high-quality diffraction images in seconds or less [19]. Figure 5(a) shows that there is a compromise between the charge that the beam line lets through and the bunch duration. In Fig. 5, the color bar represents the opening of the first slit along the x direction, and Fig. 5(a) shows that, by opening the slit, the final beam has more charge at the expense of a longer duration. This indicates that this slit can be used as a knob for the beam charge and its duration. Figures 5(b) and 5(c) show the coherence lengths L_{cx} and L_{cy}, respectively, versus charge for various optimized beam lines. The coherence length reaches a few nanometers in all cases. Here again, beams with a smaller charge lead to a higher coherence length and the slit size appears to provide some level of tunability.

Figure 6(a) shows the rms beam size through the beam line in a typical optimized configuration. The first slit, in conjunction with the first two quadrupoles, delivers a near collimated beam inside the bend magnet, with a small

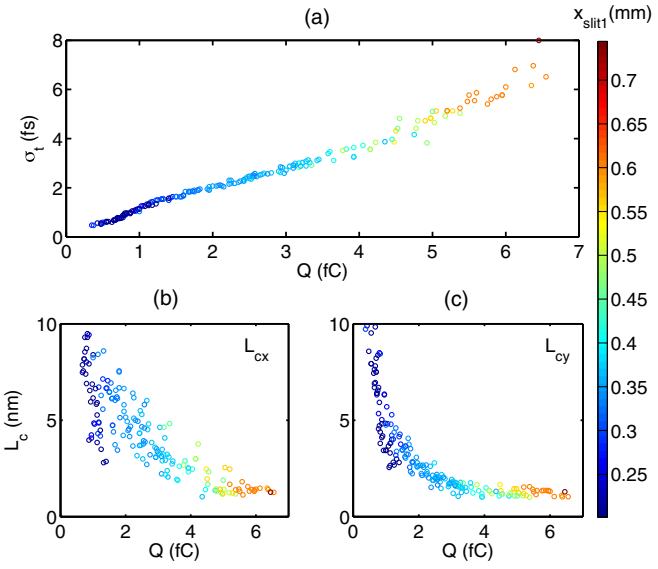

FIG. 5. Results of genetic optimization using the GPT code. (a) Optimized configurations after convergence of the algorithm showing the rms duration of the bunch σ_t versus its charge Q. (b) and (c) show the coherence lengths L_{cx} and L_{cy} versus charge for optimized configurations of the beam line. The color scheme represents the opening along x of the first slit in the beam line.

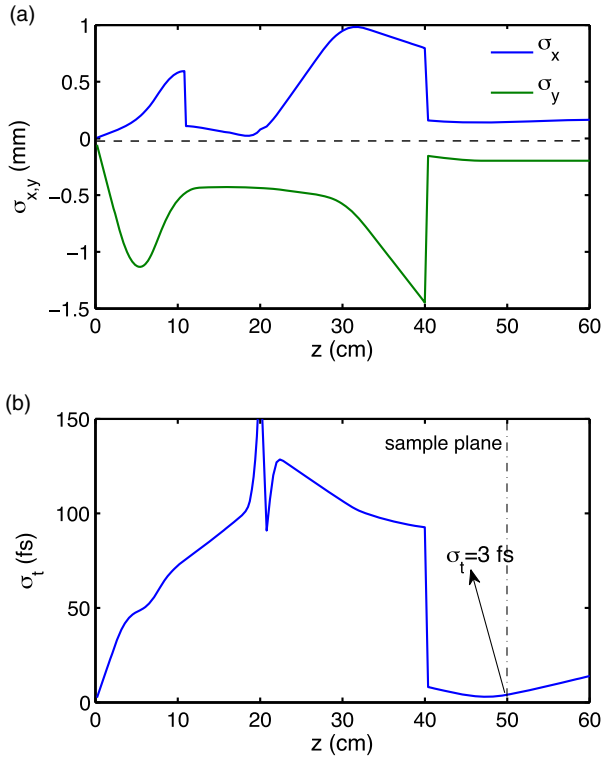

FIG. 6. Results of GPT simulations with the model distribution (see Table I). (a) rms transverse beam sizes of the beam envelope through the beam line: σ_x (blue line) and σ_y (green line). (b) rms bunch duration σ_t through the beam line. The discontinuity at $z = 20$ cm is an artifact of the rms calculation due to a change of reference frame during propagation in the bend magnet.

transverse size along x. This reduces transverse effects in the bend magnet and permits longitudinal compression of the bunch. Longitudinal dynamics is plotted in Fig. 6(b), where the blue line represents the rms bunch duration. The second slit trims the distribution even more and eliminates electrons with larger angles and traverse positions. This results in compression to sub-10-fs in the sample plane and a beam size in the 100 μm range. Without the second slit, the bunch duration would be in the 100-fs range so that a gain of one order of magnitude is achieved at the expense of a loss of charge by more than an order of magnitude.

Finally, the compression beam line also performs well when using the distribution from the PIC simulations as an input for GPT. For the simulation with the PIC distribution, space charge was taken into account throughout the whole propagation [42]. Therefore, the whole beam line, from the generation of the electron beam to its propagation and transport, is simulated numerically without any extra assumptions. Figure 7 confirms that the compression concept is still valid when using the real PIC distribution: Fig. 7(a) shows the particle distribution in longitudinal phase space, whereas Fig. 7(b) shows the temporal distribution of the electron bunch demonstrating that a bunch of 5.6 fs at FWHM and containing 1.2 fC can be achieved.

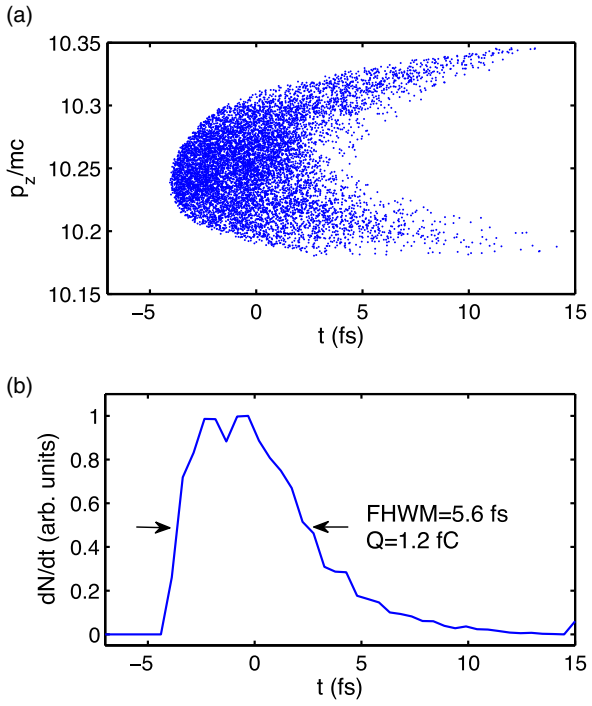

FIG. 7. Results of GPT simulations using the electron distribution from the PIC simulations. (a) Electron distribution in phase space (p_z, t) for the compressed bunch in the sample plane. (b) Temporal distribution of the bunch containing a charge of 1.2 fC. The bunch is 5.6 fs at FWHM.

We found that space charge has a minor impact on the results, apart from decreasing the transmitted charge by about 10%.

All the parameters of the input beam distribution are given in Table I. The table also shows the parameters of the distribution in the sample plane. It is clear that the distribution in the sample plane is relatively independent of the input, showing that the beam line effectively trims the beam and provides the target parameters in terms of beam size and coherence length. Finally, the transmission of the beam line is less than 1% and provides femtocoulomb charge, which is enough for performing electron diffraction [19,33]. However, the transmission could be further improved by decreasing the divergence angle at the source which might be possible using plasma lensing techniques [43] or very strong quadrupoles [44]. In this case, a charge of tens of femtocoulombs might become available.

V. CONCLUSION

In conclusion, using numerical simulations, we have demonstrated that a 5 MeV electron beam can be generated in a laser-plasma accelerator driven by a kilohertz-class laser system. In the plasma, the electron bunches have durations of a few femtoseconds. Subsequently, we have shown a simple but effective beam line that is capable of (a) trimming undesired parts of phase space, while (b) recompressing the remaining part of the beam temporally, while (c) focusing the beam on a target such that it is useful for ultrafast electron diffraction experiments. The main advantages of the proposed laser-based approach are ultrashort pulse duration, elimination of rf jitter, simplicity of the beam line, and quality of the beam. The sub-10-fs pulse duration in combination with a femtocoulomb charge on a ~100 μm spot with a transverse coherence length of 4 nm makes the electron source very relevant for ultrafast electron diffraction experiments.

ACKNOWLEDGMENTS

This work was funded by the European Research Council under Contract No. 306708, ERC Starting Grant FEMTOELEC.

[1] E. Esarey, C. B. Schroeder, and W. P. Leemans, Rev. Mod. Phys. **81**, 1229 (2009).
[2] J. Faure, Y. Glinec, A. Pukhov, S. Kiselev, S. Gordienko, E. Lefebvre, J.-P. Rousseau, F. Burgy, and V. Malka, Nature (London) **431**, 541 (2004).
[3] C. G. R. Geddes, C. Tóth, J. van Tilborg, E. Esarey, C. B. Schroeder, D. Bruhwiler, C. Nieter, J. Cary, and W. P. Leemans, Nature (London) **431**, 538 (2004).
[4] S. P. D. Mangles *et al.*, Nature (London) **431**, 535 (2004).
[5] X. Wang *et al.*, *Nat. Commun.* **4**, 1988 (2013).
[6] W. P. Leemans *et al.*, Phys. Rev. Lett. **113**, 245002 (2014).
[7] J. Faure, C. Rechatin, A. Norlin, A. Lifschitz, Y. Glinec, and V. Malka, Nature (London) **444**, 737 (2006).
[8] C. G. R. Geddes, K. Nakamura, G. R. Plateau, C. Tóth, E. Cormier-Michel, E. Esarey, C. B. Schroeder, J. R. Cary, and W. P. Leemans, Phys. Rev. Lett. **100**, 215004 (2008).
[9] K. Schmid, A. Buck, C. M. S. Sears, J. M. Mikhailova, R. Tautz, D. Herrmann, M. Geissler, F. Krausz, and L. Veisz, Phys. Rev. Spec. Top. Accel. Beams **13**, 091301 (2010).
[10] C. McGuffey *et al.*, Phys. Rev. Lett. **104**, 025004 (2010).
[11] A. Pak, K. A. Marsh, S. F. Martins, W. Lu, W. B. Mori, and C. Joshi, Phys. Rev. Lett. **104**, 025003 (2010).
[12] C. Rechatin, J. Faure, A. Ben-Ismail, J. Lim, R. Fitour, A. Specka, H. Videau, A. Tafzi, F. Burgy, and V. Malka, Phys. Rev. Lett. **102**, 164801 (2009).
[13] O. Lundh *et al.*, Nat. Phys. **7**, 219 (2011).
[14] A. R. Maier, A. Meseck, S. Reiche, C. B. Schroeder, T. Seggebrock, and F. Grüner, Phys. Rev. X **2**, 031019 (2012).
[15] Z. Huang, Y. Ding, and C. B. Schroeder, Phys. Rev. Lett. **109**, 204801 (2012).
[16] A. Loulergue, M. Labat, C. Evain, C. Benabderrahmane, V. Malka, and M.-E. Couprie, New J. Phys. **17**, 023028 (2015).
[17] R. J. D. Miller, Science **343**, 1108 (2014).
[18] A. H. Zewail and J. M. Thomas, *4D Electron Microscopy* (Imperial College Press, London, 2009).
[19] G. Sciaini and R. J. D. Miller, Rep. Prog. Phys. **74**, 096101 (2011).

[20] T. van Oudheusden, P. L. E. M. Pasmans, S. B. van der Geer, M. J. de Loos, M. J. van der Wiel, and O. J. Luiten, Phys. Rev. Lett. **105**, 264801 (2010).
[21] P. Musumeci, J. T. Moody, C. M. Scoby, M. S. Gutierrez, and M. Westfall, Appl. Phys. Lett. **97**, 063502 (2010).
[22] http://www.pulsar.nl/gpt.
[23] J. B. Hastings, F. M. Rudakov, D. H. Dowell, J. F. Schmerge, J. D. Cardoza, J. M. Castro, S. M. Gierman, H. Loos, and P. M. Weber, Appl. Phys. Lett. **89**, 184109 (2006).
[24] Y. Murooka, N. Naruse, S. Sakakihara, M. Ishimaru, J. Yang, and K. Tanimura, Appl. Phys. Lett. **98**, 251903 (2011).
[25] P. Musumeci, J. T. Moody, C. M. Scoby, M. S. Gutierrez, H. A. Bender, and N. S. Wilcox, Rev. Sci. Instrum. **81**, 013306 (2010).
[26] V. Malka *et al.*, Phys. Plasmas **8**, 3467 (2001).
[27] E. Guillaume *et al.*, Phys. Rev. Spec. Top. Accel. Beams **18**, 061301 (2015).
[28] A. Pukhov and J. Meyer-ter-Vehn, Appl. Phys. B **74**, 355 (2002).
[29] W. Lu, M. Tzoufras, C. Joshi, F. S. Tsung, W. B. Mori, J. Vieira, R. A. Fonseca, and L. O. Silva, *Phys. Rev. Accel. Beams* **10**, 061301 (2007).
[30] S. Bohman, A. Suda, T. Kanai, S. Yamaguchi, and K. Midorikawa, Opt. Lett. **35**, 1887 (2010).
[31] F. Böhle *et al.*, Laser Phys. Lett. **11**, 095401 (2014).
[32] Z.-H. He, B. Hou, J. H. Easter, J. Faure, K. Krushelnick, J. A. Nees, and A. G. R. Thomas, New J. Phys. **15**, 053016 (2013).
[33] Z.-H. He, A. G. R. Thomas, B. Beaurepaire, J. A. Nees, B. Hou, V. Malka, K. Krushelnick, and J. Faure, Appl. Phys. Lett. **102**, 064104 (2013).
[34] A. J. Goers, G. A. Hine, L. Feder, B. Miao, F. Salehi, J. K. Wahlstrand, and H. M. Milchberg, Phys. Rev. Lett. **115**, 194802 (2015).
[35] M. Thevenet, A. Leblanc, S. Kahaly, H. Vincenti, A. Vernier, F. Quere, and J. Faure, *Nat. Phys.* (to be published).
[36] A. Lifschitz, X. Davoine, E. Lefebvre, J. Faure, C. Rechatin, and V. Malka, J. Comput. Phys. **228**, 1803 (2009).
[37] B. Beaurepaire, A. Lifschitz, and J. Faure, New J. Phys. **16**, 023023 (2014).
[38] S. Tokita, S. Inoue, S. Masuno, M. Hashida, and S. Sakabe, Appl. Phys. Lett. **95**, 111911 (2009).
[39] P. Kung, H.-c. Lihn, H. Wiedemann, and D. Bocek, Phys. Rev. Lett. **73**, 967 (1994).
[40] A. W. Chao and M. Tigner, *Handbook of Accelerator Physics and Engineering* (World Scientific, London, 1999).
[41] B. D. Muratori, J. K. Jones, and A. Wolski, arXiv: 1404.1762.
[42] G. Pöplau, U. van Rienen, B. van der Geer, and M. de Loos, IEEE Trans. Magn. **40**, 714 (2004).
[43] C. Thaury *et al.*, Nat. Commun. **6**, 6860 (2015).
[44] T. Eichner, F. Grüner, S. Becker, M. Fuchs, D. Habs, R. Weingartner, U. Schramm, H. Backe, P. Kunz, and W. Lauth, Phys. Rev. Spec. Top. Accel. Beams **10**, 082401 (2007).